Journal of Applied Physics ARTICLE pubs.aip.org/aip/jap

The impact of device length on the electron's effective mobility

Cite as: J. Appl. Phys. **134**, 125701 (2023); doi: 10.1063/5.0171559
Submitted: 9 August 2023 · Accepted: 13 September 2023 ·
Published Online: 28 September 2023

Alireza Azimi,[1] Mohammadreza Azimi,[1] Michael S. Shur,[2] and Stephen K. O'Leary[1,a)]

AFFILIATIONS

[1]School of Engineering, The University of British Columbia, Kelowna, British Columbia V1V 1V7, Canada
[2]Electrical, Computer, and Systems Engineering, Rensselaer Polytechnic Institute, Troy, New York 12180, USA

[a)]**Author to whom correspondence should be addressed:** stephen.oleary@ubc.ca

ABSTRACT

Within the framework of an electron transport regime classification scheme, we aim to explore the boundaries that occur between the ballistic, collision-dominated, space-charge injection, and non-space-charge injection electron transport regimes that are experienced by an electron within a semiconducting device, mapping out where these different electron transport regimes are. We do this by determining the electron's mean free path and the relevant screening length. In order to make this analysis concrete, we perform this analysis for four representative semiconductor material systems, including silicon, gallium arsenide, the 4H-phase of silicon carbide, and the wurtzite phase of gallium nitride. The entire analysis is performed using a two-dimensional approach, this being representative of the electron transport that is experienced by an electron in the vicinity of a two-dimensional electron gas. Finally, following an evaluation of the dependence of the ballistic mobility on the device length scale for all four materials, an evaluation of the effective mobility as a function of the channel-length scale is pursued, a Matthiessen-rule based approach being employed for the purposes of this analysis.

I. INTRODUCTION

Driven by the expectations set-out in Moore's law, thus far, the microelectronics industry has sought to advance its technologies primarily through reductions in the feature-length scale.[1–4] This scaling approach to technological development has served the silicon (Si) dominated industry very well for many years, with remarkable progress being made, both at increasing the integration density and in enhancing computational capacity.[5,6] Unfortunately, Si-based technologies have now almost reached their projected scale limit, i.e., 5 nm, this limit being set by short-channel effects, i.e., the presence of direct electron tunneling between the source and the drain and degradation in the gate control over the channel.[7] This has encouraged the community to consider alternate materials and novel device configurations, impressively short gate lengths recently being realized in a variety of other material systems, including carbon nanotube-based transistors with gate lengths as short as 2.8 nm[8] and MoS_2-based transistors with 1 nm gate lengths.[9]

Device scale reductions will inevitably introduce new features into the electron transport calculus that are not important when the devices are of a larger scale. Shur and Eastman[10] posit that the conventional collision-dominated based electron transport perspective is only relevant when the device scale is large when contrasted with the mean free path of an electron, λ. For devices with feature-length scales, L, less than λ, however, the electrons transiting the device will not have the time required in order to achieve steady-state. Accordingly, they will behave ballistically during their transit across the device. Later on, Lee and Shur[11] further enriched this electron transport perspective by differentiating between L being shorter or longer than the relevant screening length, L_D, devices with L shorter than L_D experiencing space-charge injection, while devices with L longer than L_D experience negligible space-charge injection. The quartet of electron transport possibilities that arise from the permutations in these possibilities, i.e., whether L is shorter or longer than both λ and L_D, leads to an electron transport classification scheme that represents the various possible electron transport conduction conditions experienced by electrons within an electron device; see Fig. 1. For the purposes of this analysis, we ascribe a numbering scheme to the quadrants in this electron transport classification scheme, regime I corresponding to ballistic electron transport with space-charge injection, regime II corresponding to collision-dominated electron transport with space-charge

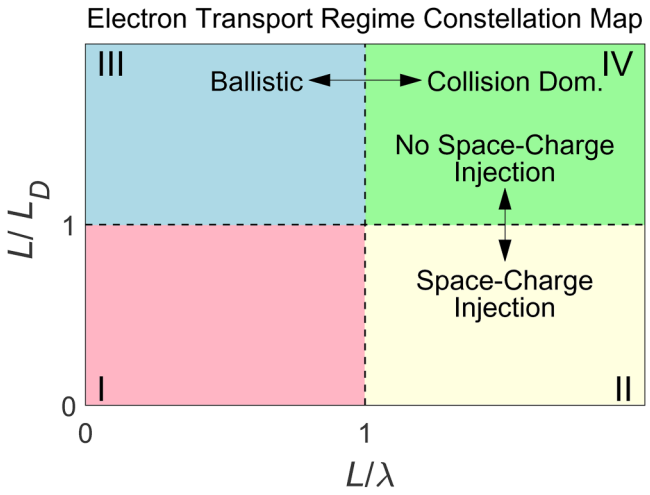

FIG. 1. The electron transport regime constellation map. Regime I corresponds to ballistic electron transport with space-charge injection, regime II corresponds to collision-dominated electron transport with space-charge injection, regime III corresponds to ballistic electron transport without space-charge injection, and regime IV corresponds to collision-dominated electron transport without space-charge injection. The online version is in color.

injection, regime III corresponding to ballistic electron transport without space-charge injection, and regime IV corresponding to collision-dominated electron transport without space-charge injection. This electron transport classification scheme, which we alternatively refer to as an electron transport regime constellation map, embodies the spirit of the electron transport classification scheme proposed by Lee and Shur.[11] While in reality, of course, the boundaries between these various regimes are expected to be quite porous, the electron transport regime constellation map provides us with a useful organizational structure within which we can frame the subsequent analysis.

While the presence of ballistic electron transport within short-channel devices was accepted by many within the electron device community,[12,13] when first proposed some reserved judgment on the validity of this concept. This skepticism was ultimately overcome when direct experimental evidence was presented demonstrating ballistic electron transport within thin gallium arsenide (GaAs) layers.[14] Since then, ballistic electron transport related interpretations have been widely used by researchers working with short-channel device acquired experimental data sets. Key developments in this field include, but are certainly not limited to, the work of Natori,[15] in which an expression for the current experienced by a ballistic n-channel MOSFET was determined, Lundstrom *et al.*,[16,17] in which a quantum theory of ballistic electron transport was developed, Kastalsky and Shur,[18] in which the concept of ballistic mobility was introduced, this concept being further developed by Dmitriev and Shur,[19] and Antoniadis,[20] in which a ballistic electron transport related theory was developed that allows one to determine the effective mobility as a function of the channel-length scale. Work building upon this ballistic electron transport concept continues to be performed to this very day.

We would like to explore whether or not the electron transport regime constellation map provided in Fig. 1 provides the community with a frame of reference that can be used to interpret the role of ballistic electron transport. Unfortunately, thus far, the electron transport constellation map has really only been used to qualitatively interpret electron transport possibilities. Unfortunately, this has rendered this concept a difficult one to use by members of the broader electron device community who have a preference for quantitative benchmarks. Accordingly, in this paper, we will quantitatively explore the boundaries between the various quadrants in the electron transport regime constellation map. We do this through an evaluation of the electron's mean free path, λ, and a determination of the relevant screening length, L_D. In order to make this analysis concrete, we perform this analysis for four representative semiconductor material systems, including Si and gallium arsenide (GaAs), these being traditional semiconducting materials, the 4H-phase of silicon carbide (4H-SiC), a material often used in high-power semiconductor devices,[21,22] and the wurtzite phase of gallium nitride (W-GaN), this material being representative of that found in modern high electron mobility transistors.[23,24] Finally, following an evaluation of the dependence of the ballistic mobility on L for all four materials, an evaluation of the effective mobility as a function of L will be pursued, the goal being to explore what happens to the effective mobility as L approaches the bulk limit; a Matthiessen's-rule based formalism is employed in the effective mobility evaluations, as was pursued earlier by Shur[25] and Chilleri *et al.*[26] While the analyzes of Shur[25] and Chilleri *et al.*[26] were performed within the framework of a three-dimensional approach, here the entire analysis is performed using a two-dimensional approach, this being representative of the electron transport that is experienced by an electron in the vicinity of a two-dimensional electron gas (2DEG).[27–29]

This paper is organized in the following manner. In Sec. II, the relevant material parameters are introduced and the momentum relaxation times are plotted as functions of the drift mobility for all of the materials considered in this analysis. Then, in Sec III, the mean free paths and screening length evaluations are performed. With these evaluations completed, in Sec. IV, a comparison between the different materials is offered, the goal being to see where each material sits in reference to the electron transport regime constellation map. In Sec. V, following an evaluation of the dependence of the ballistic mobility on the device length scale for all four materials, an evaluation of the effective mobility as a function of the channel-length scale is pursued, a Matthiessen-rule based approach being employed for the purposes of this analysis. Finally, the conclusions of this analysis are featured in Sec. VI.

II. MATERIAL PARAMETER SELECTION

In order to perform this analysis, we must specify the relevant material parameters corresponding to the suite of semiconductor materials under consideration, i.e., Si, GaAs, 4H-SiC, and W-GaN. The electron effective mass, m^*, the relative dielectric constant of the material itself, ϵ_r, and the relative dielectric constant of the passivation layer that might be included in a conceivable device configuration, ϵ_p, are the relevant material parameters required in order to perform the proposed computations; as will be seen later on, ϵ_r

and ϵ_p are required for the L_D evaluations, our selection of passivation layers corresponding to a specific potential device configuration. The 300 K maximum mobility value, $\mu_{max.}$, which of course will be chiefly determined by the corresponding intrinsic mobility, provides a benchmark in this analysis, many of the results being plotted as a function of the electron drift mobility, μ. The material parameter selections drawn upon for the purposes of this analysis are tabulated in Table I.[30–33]

We start the analysis by plotting the momentum relaxation time, τ, as a function of the drift mobility, μ, for all of the materials considered in this analysis. We perform this analysis by observing that the drift mobility,

$$\mu = \frac{q\,\tau}{m^*}, \tag{1}$$

q being the electron charge, all other parameters being as previously defined. This dependence is shown in Fig. 2, for the specific case of the crystal temperature being set to 300 K. It is noted that for a set nominal drift mobility value of 500 $cm^2/V\,s$, the momentum relaxation times are 54.0, 17.9, 119.4, and 56.9 fs, for the cases of Si, GaAs, 4H-SiC, and W-GaN, respectively. At the 300 K maximum mobility value, $\mu_{max.}$, the momentum relaxation times are 152.2, 304.5, 214.9, and 113.7 fs, for the cases of Si, GaAs, 4H-SiC, and W-GaN, respectively. In Fig. 2, for each material, the point at which the 300 K maximum mobility value, $\mu_{max.}$, is achieved is marked with a symbol and corresponds to when the transition from the solid line to the dashed line occurs. Extensions into the dashed line regions are expected to have physical meaning for the case of cooler temperature selections and non-bulk conditions, such as those that might be expected to occur in the vicinity of a 2DEG.

TABLE I. A tabulation of the relevant material parameters corresponding to the materials under investigation, i.e., Si, GaAs, 4H-SiC, and W-GaN. Material parameters tabulated include the 300 K maximum mobility value, $\mu_{max.}$, the electron effective mass, m^*, the relative dielectric constant of the material itself, ϵ_r, and the relative dielectric constant of the passivation layer that might be included in a conceivable device configuration, ϵ_p, the material from which this passivation layer might be fabricated also being indicated. The 300 K maximum mobility value, $\mu_{max.}$, the electron effective mass, m^*, the relative dielectric constant of the material itself, ϵ_r, and the relative dielectric constant of the passivation layer, ϵ_p, are estimated from the relevant scientific literature. The free electron mass is denoted with m_e. We focused on the material parameter selections identified in the handbook series of Levinshtein *et al.*[30–33]

Material	$\mu_{max.}$ at 300 K ($cm^2/V\,s$)	m^*	ϵ_r	ϵ_p (passivation material)
Si	1400[30]	0.19 m_e[30,a]	11.7[30]	3.9 (SiO_2)
GaAs	8500[31]	0.063 m_e[31]	12.9[31]	11.0 (AlGaAs)
4H-SiC	900[32]	0.42 m_e[32,a]	9.66[32,b]	3.9 (SiO_2)
W-GaN	1000[33]	0.20 m_e[33]	8.9[33]	9.0 (AlGaN)

[a]The transverse effective mass selected.
[b]The perpendicular dielectric constant selected.

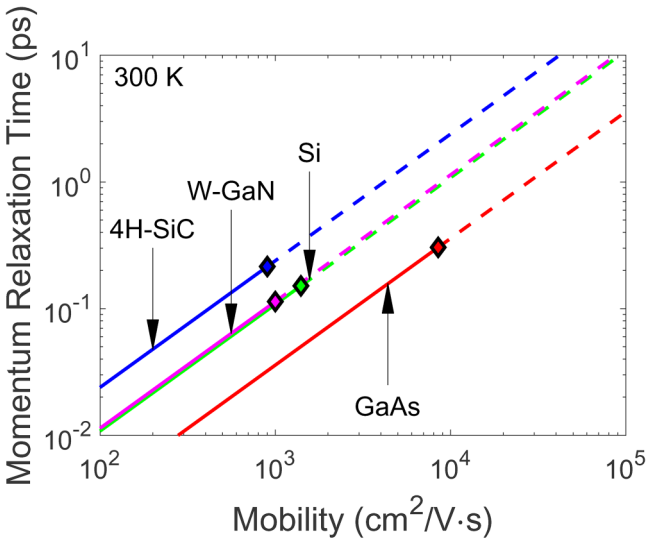

FIG. 2. The dependence of the momentum relaxation time on the mobility for the cases of Si, GaAs, 4H-SiC, and W-GaN. The material parameters employed for the purposes of this analysis are those tabulated in Table I. For each material, the point at which the 300 K maximum mobility value, $\mu_{max.}$, is achieved is marked with a symbol and corresponds to where the transition, from solid line to dashed line, occurs. The online version is in color.

III. MEAN FREE PATH AND SCREENING LENGTH EVALUATIONS

In an effort to estimate the mean free path of an electron, λ, we pursue the course of analysis prescribed by Shur and Eastman,[10] setting

$$\lambda = \tau\, v_{th.}, \tag{2}$$

where $v_{th.}$ denotes the corresponding thermal velocity, τ being as previously defined. For the case of two-dimensional electron transport, it can be shown that

$$v_{th.} = \sqrt{\frac{\pi k_B T}{2m^*}}, \tag{3}$$

where T denotes the crystal temperature, k_B represents the Boltzmann constant, and m^* is as defined earlier.[19] From Eqs. (1) and (3), it is noted that Eq. (2) may alternatively be expressed as

$$\lambda = \frac{\mu}{q}\sqrt{\frac{\pi k_B T m^*}{2}}, \tag{4}$$

where all terms are as previously defined. In Fig. 3, we plot the dependence of λ on the drift mobility value, μ, for the various materials, i.e., Si, GaAs, 4H-SiC, and W-GaN, for the case of the crystal temperature set to 300 K. Setting the drift mobility value to its nominal value, i.e., 500 $cm^2/V\,s$, the mean free paths of an electron are determined to be 10.5, 6.0, 15.6, and 10.7 nm, for the cases

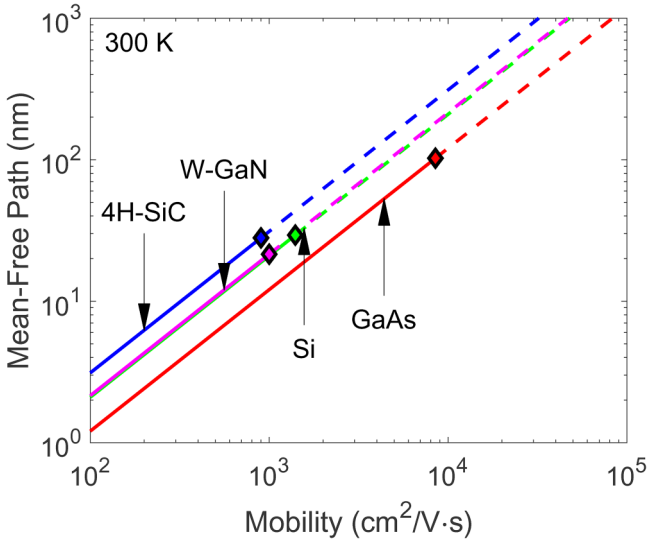

FIG. 3. The electron's mean free path, λ, as a function of the electron mobility, μ, for the various materials considered, i.e., Si, GaAs, 4H-SiC, and W-GaN. This result is determined using Eq. (4) for the crystal temperature set to 300 K. For each material, the point at which the 300 K maximum mobility value, $\mu_{max.}$, is achieved is marked with a symbol and corresponds to where the transitions, from solid line to dashed line, occur. The online version is in color.

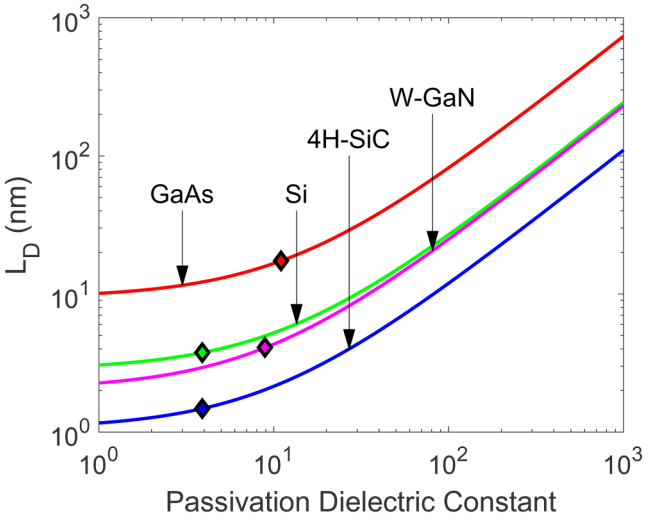

FIG. 4. The two-dimensional screening length, L_D, as a function of the relative passivation layer dielectric constant, ϵ_p, for the various materials considered, i.e., Si, GaAs, 4H-SiC, and W-GaN. This result is determined using Eqs. (5) and (6). The screening length evaluations, corresponding to the specific passivation dielectric constant values suggested in Table I, are shown with the solid symbols. The online version is in color.

of Si, GaAs, 4H-SiC, and W-GaN, respectively. For the 300 K maximum mobility values, $\mu_{max.}$, the corresponding λ values are found to be 29.3, 102.5, 28.0, and 21.5 nm, for the cases of Si, GaAs, 4H-SiC, and W-GaN, respectively, these being beyond the minimum device feature-length scale found in contemporary electron devices. Accordingly, we conclude that ballistic transport is expected to play a significant role in shaping the performance of short devices fabricated from these materials.

The evaluation of the screening length, L_D, for the two-dimensional case is not as straightforward as its three-dimensional counterpart, the Debye length being the screening length for the three-dimensional case. In fact, it can be shown that the space-charge injection that occurs from a 2DEG into a region of lower concentration attenuates quite slowly in comparison with the three-dimensional case, the details being intimately connected with the device geometry employed. Within the framework of an n_+–n_o–n_+ device structure, Dmitriev and Shur[34] were able to evaluate the two-dimensional screening length, L_D, for this particular device geometry. Building upon this analytical framework, neglecting one of the terms in the expressions of Dmitriev and Shur[34] which is of secondary importance, we find that the two-dimensional screening length may be approximately expressed as

$$L_D = e\frac{2a_B^{'}}{\pi}, \tag{5}$$

where e denotes Euler's number and where the effective Bohr radius

$$a_B^{'} = (\epsilon_r + \epsilon_p)\frac{4\pi\epsilon_o\hbar^2}{2q^2m^*}, \tag{6}$$

where ϵ_o denotes the dielectric constant associated with vacuum and $\hbar$ represents the reduced Planck's constant, all other terms being as defined earlier; the conjuncture of Eqs. (5) and (6), which apply when the length scale exceeds $a_B^{'}$, produce results that are very similar, i.e., within a couple of percentage points, to that of Dmitriev and Shur.[34] In Fig. 4, we plot L_D, as prescribed in Eqs. (5) and (6), as a function of the passivation layer's relative dielectric constant, i.e., ϵ_p, for the different materials involved in this analysis. It is noted that this approximate result, determined through the conjuncture of Eqs. (5) and (6), produces results that are very similar to those presented in Fig. 4 of Dmitriev and Shur,[34] suggesting that the approximate result is perfectly adequate for our particular purposes. It is noted that for the passivation layer selections suggested in Table I, the resultant L_D values are 3.8, 17.4, 1.5, and 4.1 nm for the cases of Si, GaAs, 4H-SiC, and W-GaN, respectively.

IV. COMPARISON BETWEEN MATERIALS

With our evaluations of λ and L_D complete, we are now ready to comment on where each material sits in reference to the electron transport regime constellation map presented in Fig. 1. Representative evaluations of these quantities are tabulated in Table II; in order to make our evaluations concrete, we focused on the evaluations performed for λ for the case of the 300 K maximum mobility values, $\mu_{max.}$, and for L_D for the suggested ϵ_p value suggested in Table I. For these particular evaluations, we note

TABLE II. A tabulation of the electron's mean free path, λ, evaluated at the 300 K maximum mobility value, $\mu_{max.}$, and the screening length, L_D, evaluated for the passivation layer relative dielectric constant value, ϵ_p, tabulated in Table I, corresponding to the materials under investigation, i.e., Si, GaAs, 4H-SiC, and W-GaN.

Material	λ at $\mu_{max.}$ (nm)	L_D at ϵ_p (nm) (passivation material)
Si	29.3	3.8 (SiO_2)
GaAs	102.5	17.4 (AlGaAs)
4H-SiC	28.0	1.5 (SiO_2)
W-GaN	21.5	4.1 (AlGaN)

that for all of the materials considered in this analysis that L_D is shorter than λ. This implies that only regime II of the electron transport regime constellation map is not accessible by these materials, which corresponds to a collision-dominated electron transport regime with space-charge injection. In Fig. 5, the extent of the various electron transport regimes is schematically illustrated for the various materials considered. It is noted GaAs experiences a much longer ballistic electron transport range when compared with the other materials. Its light effective mass, m^*, and high 300 K maximum mobility value, $\mu_{max.}$, are the principal factors responsible for this.

V. BALLISTIC ELECTRON TRANSPORT AND DETERMINATION OF THE EFFECTIVE MOBILITY

When an electron experiences ballistic electron transport, Dmitriev and Shur[19] have found it instructive to introduce the concept of ballistic mobility,

$$\mu_{ball.} = \alpha \frac{q\,L}{m^*\,v}, \tag{7}$$

which is seen to linearly increase with the device feature-length scale, L, v being set to the thermal velocity, i.e., $v_{th.}$ as presented in Eq. (3), for the case of non-degenerate statistics, α being a constant of the order of unity, all other terms being as previously defined; a detailed analysis demonstrates that for the case of two-dimensional electron transport that α is $\frac{1}{2}$ for the non-degenerate case. The ballistic mobility is plotted as a function of L for the various materials considered for the non-degenerate case in Fig. 6, i.e., for v set to $v_{th.}$ as prescribed in Eq. (3). These computations are performed for the crystal temperature set to 300 K. As can be seen from Fig. 6, the ballistic mobility linearly scales with L, a doubling of the device length corresponding to a doubling of the ballistic mobility. For a nominal device length selection of 100 nm, the ballistic mobility values are found to be 2390, 4150, 1610, and 2330 $cm^2/V\,s$, for the cases of Si, GaAs, 4H-SiC, and W-GaN, respectively.

Finally, we connect this ballistic mobility concept with the measured effective mobility, $\mu_{eff.}$, found in an actual electron device. Through the use of Matthiessen's-rule, it can be crudely argued that

$$\frac{1}{\mu_{eff.}} = \frac{1}{\mu_{ball.}} + \frac{1}{\mu_o}, \tag{8}$$

where μ_o corresponds to the conventional low-field collision-

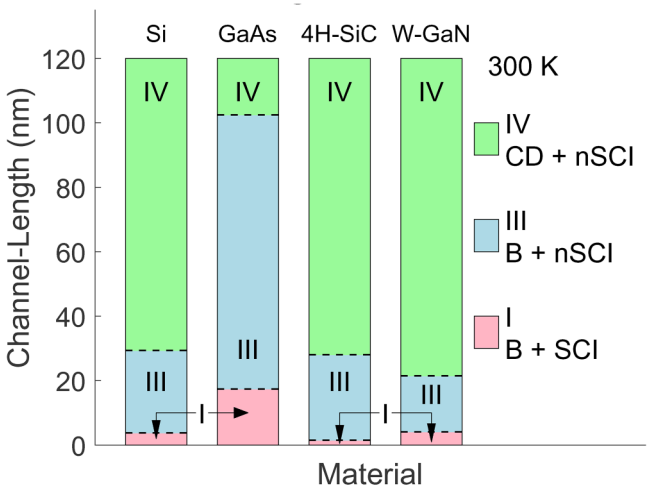

FIG. 5. The various electron transport regimes, as defined by the electron transport regime constellation map, corresponding to the various materials considered, i.e., Si, GaAs, 4H-SiC, and W-GaN. The electron transport regimes are as defined in the electron transport regime constellation map, i.e., Fig. 1. The classification scheme categories, and the numbering scheme indicated here, are exactly the same as shown in Fig. 1. The various aspects of electron transport, i.e., ballistic (B), collision-dominated (CD), space-charge injection (SCI), and non-space-charge injection (nSCI), are shown. The online version is in color.

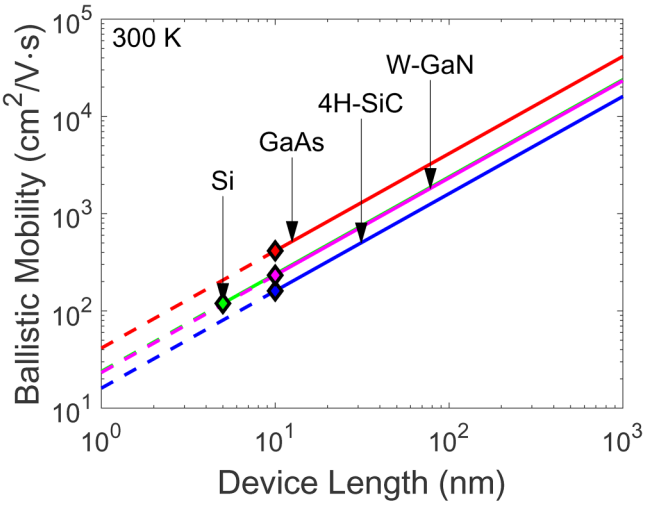

FIG. 6. The ballistic mobility, $\mu_{ball.}$, as a function of the device length, L, as evaluated through the use of Eq. (7), for the materials considered, i.e., Si, GaAs, 4H-SiC, and W-GaN. The non-degenerate form of ballistic mobility, $\mu_{ball.}$, is employed for the purposes of this analysis. The crystal temperature is set to 300 K for these computations. The solid lines are extended to 5 nm for the case of Si and 10 nm for the cases of the other materials. For each material, the transition between the solid and dashed lines is marked with a symbol. The online version is in color.

dominated mobility, i.e., the bulk mobility.[35–37] In order to appreciate the impact that ballistic mobility plays in shaping the effective mobility as L transitions from the ballistic to the collision-dominated electron transport regimes, in Fig. 7, we plot the dependence of the effective mobility, $\mu_{\text{eff.}}$, on the device feature-length scale, L, for the materials considered. Once again, we perform these computations for the crystal temperature set to 300 K. In order to make the analysis concrete, we set the bulk mobility values, μ_o, to the 300 K maximum mobility value for each material considered in this analysis, $\mu_{\text{max.}}$, these values being tabulated in Table I. The range of device lengths, i.e., L, was selected to range the gamut from 1 to 1000 nm, this corresponding to the range of device lengths that can be found in some modern electron devices.[9,38] We perform these computations using the non-degenerate form of ballistic mobility, i.e., we set ν to $\nu_{\text{th.}}$ as prescribed in Eq. (3). It is noted that for the shorter device lengths, the ballistic mobility dominates the effective mobility; note the similarity in the results presented in Figs. 6 and 7 for L selections less than 10 nm. The transition to the collision-dominated regime leads to an eventual saturation in the monotonic increase in the effective mobility as the device length is increased, the bulk mobility result, μ_o, being achieved in the bulk limit. It is noted that the transition to the bulk limit seems slowest for the case of GaAs. Considering that GaAs also has the longest electron mean free path compared with the other materials, this seems reasonable; the λ values, evaluated at the 300 K maximum mobility value, i.e., $\mu_{\text{max.}}$, for each material considered, are also indicated in Fig. 7.

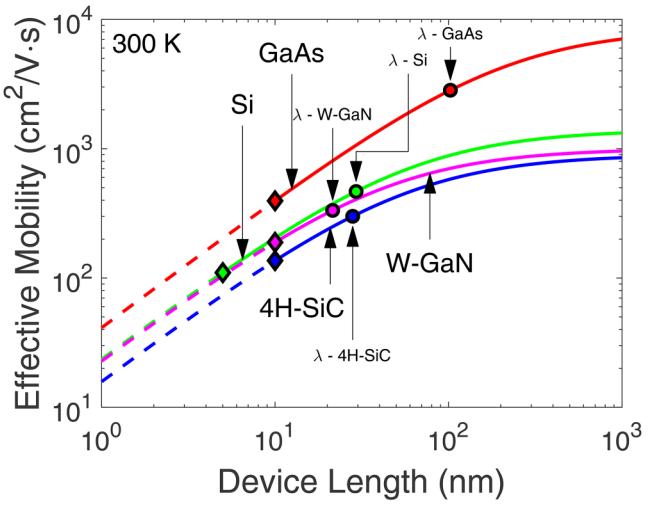

FIG. 7. The effective mobility, $\mu_{\text{eff.}}$, as a function of the device length, L, as evaluated through the use of Eq. (8), for the materials considered, i.e., Si, GaAs, 4H-SiC, and W-GaN. The non-degenerate form of ballistic mobility, $\mu_{\text{ball.}}$, is employed. The bulk mobility selections are set to the 300 K maximum mobility values, $\mu_{\text{max.}}$, prescribed in Table I. The effective mobility, $\mu_{\text{eff.}}$, is determined through the use of Eq. (8). The crystal temperature is set to 300 K for these computations. The solid lines are extended to 5 nm for the case of Si and 10 nm for the cases of the other materials. For each material, the transition between the solid and dashed lines is marked with a symbol. The electron's mean free path, evaluated for the 300 K maximum mobility value, $\mu_{\text{max.}}$, is also indicated for all materials considered. The online version is in color.

VI. CONCLUSIONS

In conclusion, we aimed to explore the boundaries that occur between the ballistic, collision-dominated, space-charge injection, and non-space-charge injection electron transport regimes that are experienced by an electron within a semiconducting device, mapping out where these different electron transport regimes are. We did this through an evaluation of the electron's mean free path, λ, and a determination of the screening length, L_D, for the cases of Si, GaAs, 4H-SiC, and W-GaN. The entire analysis was performed using a two-dimensional approach, this being representative of the electron transport that may be experienced by an electron in the vicinity of a 2DEG. Finally, following an evaluation of the dependence of the ballistic mobility on device length, L, for all four materials, an evaluation of the effective mobility as a function of the channel-length scale was pursued, a Matthiessen-rule based approach being employed for the purposes of this analysis.

ACKNOWLEDGMENTS

The authors would like to acknowledge the Natural Sciences and Engineering Research Council of Canada and MITACS for financial support.

AUTHOR DECLARATIONS

Conflict of Interest

The authors have no conflicts to disclose.

Author Contributions

All of the computations were performed by Alireza Azimi, Mohammadreza Azimi, and Stephen K. O'Leary. All of the figures were produced by Alireza Azimi and Stephen K. O'Leary. The text was primarily written by Alireza Azimi and Stephen K. O'Leary, in consultation with Michael S. Shur. The work of Alireza Azimi and Mohammadreza Azimi was supervised by Stephen K. O'Leary. Michael S. Shur made some invaluable technical suggestions with respect to this manuscript, these helping shape its form and clarity.

Alireza Azimi: Formal analysis (equal); Investigation (equal); Writing – original draft (equal). **Mohammadreza Azimi:** Formal analysis (equal); Investigation (equal); Writing – original draft (equal). **Michael S. Shur:** Formal analysis (equal). **Stephen K. O'Leary:** Conceptualization (equal); Data curation (equal); Formal analysis (equal); Funding acquisition (equal); Investigation (equal); Supervision (equal); Writing – original draft (equal); Writing – review & editing (equal).

DATA AVAILABILITY

The data that support the findings of this study are available from the corresponding author upon reasonable request.

REFERENCES

[1]M. Ieong, B. Doris, J. Kedzierski, K. Rim, and M. Yang, Science **306**, 2057 (2004).
[2]R. Chau, B. Doyle, S. Datta, J. Kavalieros, and K. Zhang, Nat. Mater. **6**, 810 (2007).
[3]A. B. Kelleher, *2022 International Electron Devices Meeting Proceedings* (IEEE, 2022).
[4]M. Radosavljevic and J. Kavalieros, IEEE Spectrum **59**(12), 32 (2022).
[5]M. Bohr, Commun. ACM **41**, 80 (1998).
[6]V. Passi and J.-P. Raskin, Semicond. Sci. Technol. **32**, 123004 (2017).
[7]H. Kawaura, T. Sakamoto, and T. Baba, Appl. Phys. Lett. **76**, 3810 (2000).
[8]D.-M. Tang, S. V. Erohin, D. G. Kvashnin, V. A. Demin, O. Cretu, S. Jiang, L. Zhang, P.-X. Hou, G. Chen, D. N. Futaba, Y. Zheng, R. Xiang, X. Zhou, F.-C. Hsia, N. Kawamoto, M. Mitome, Y. Nemoto, F. Uesugi, M. Takeguchi, S. Maruyama, H.-M. Cheng, Y. Bando, C. Liu, P. B. Sorokin, and D. Golberg, Science **374**, 1616 (2021).
[9]S. B. Desai, S. R. Madhvapathy, A. B. Sachid, J. P. Llinas, Q. Wang, G. H. Ahn, G. Pitner, M. J. Kim, J. Bokor, C. Hu, H.-S. P. Wong, and A. Javey, Science **354**, 99 (2016).
[10]M. S. Shur and L. F. Eastman, IEEE Trans. Electron Devices **26**, 1677 (1979).
[11]K. Lee and M. S. Shur, J. Appl. Phys. **54**, 4028 (1983).
[12]H.-U. Habermeier, AIP Conf. Proc. **122**, 192 (1984).
[13]H. U. Baranger and J. W. Wilkins, Phys. Rev. B **30**, 7349 (1984).
[14]M. Heiblum, M. I. Nathan, D. C. Thomas, and C. M. Knoedler, Phys. Rev. Lett. **55**, 2200 (1985).
[15]K. Natori, J. Appl. Phys. **76**, 4879 (1994).
[16]M. Lundstrom, IEEE Electron Device Lett. **18**, 361 (1997).
[17]M. Lundstrom and J. Guo, *Nanoscale Transistors Device Physics, Modeling and Simulation* (Springer, New York, 2006).
[18]A. A. Kastalsky and M. S. Shur, Solid State Commun. **39**, 715 (1981).
[19]A. P. Dmitriev and M. S. Shur, Appl. Phys. Lett. **89**, 142102 (2006).
[20]D. Antoniadis, IEEE Trans. Electron Devices **63**, 2650 (2016).
[21]C. Dorfer, M. E. Bathen, S. Race, P. Kumar, A. Tsibizov, J. Woerle, and U. Grossner, Appl. Phys. Lett. **122**, 183503 (2023).
[22]P. Steinmann, B. Hull, I.-H. Ji, D. Lichtenwalner, and E. Van Brunt, J. Appl. Phys. **133**, 235705 (2023).
[23]N. Remesh, H. Chandrasekar, A. Venugopalrao, S. Raghavan, M. Rangarajan, and D. N. Nath, J. Appl. Phys. **130**, 075702 (2021).
[24]V. Joshi, R. R. Chaudhuri, S. D. Gupta, and M. Shrivastava, IEEE Trans. Electron Devices **70**, 3011 (2023).
[25]M. S. Shur, IEEE Electron Device Lett. **23**, 511 (2002).
[26]J. Chilleri, P. Siddiqua, M. S. Shur, and S. K. O'Leary, Appl. Phys. Lett. **120**, 122105 (2022).
[27]A 2DEG typically arises in the neighborhood of a heterojunction formed at the interface between two different materials. For the case of SiC, however, a 2DEG can be formed at the interface between different polytypes of this material.[28,29] While the evaluations that we perform for the 2DEG could be complicated by a variety of technical considerations, i.e., the different polytypes involved and their partial contributions to various physical properties, we perform our computations simply using the material properties associated with 4H-SiC, noting that this approach is perfectly adequate for the order of magnitude comparisons that we are performing within the scope of this analysis.
[28]M. V. S. Chandrashekhar, C. I. Thomas, J. Lu, and M. G. Spencer, Appl. Phys. Lett. **91**, 033503 (2007).
[29]H. Sazawaa and H. Yamaguchi, Appl. Phys. Lett. **120**, 212102 (2022).
[30]M. E. Levinshtein and S. L. Rumyantsev, *Silicon (Si)*, Chapter 1 in *Handbook Series on Semiconductor Parameters Volume 1: Si, Ge, C (Diamond), GaAs, GaP, GaSb, InAs, InP, InSb*, edited by M. Levinshtein, S. Rumyantsev, and M. Shur (World Scientific, River Edge, 1996).
[31]M. E. Levinshtein and S. L. Rumyantsev, *Gallium Arsenide (GaAs)*, Chapter 4 in *Handbook Series on Semiconductor Parameters Volume 1: Si, Ge, C (Diamond), GaAs, GaP, GaSb, InAs, InP, InSb*, edited by M. Levinshtein, S. Rumyantsev, and M. Shur (World Scientific, River Edge, 1996).
[32]Y. Goldberg, M. Levinshtein, and S. Rumyantsev, *Silicon Carbide (SiC)*, Chapter 5 in *Properties of Advanced Semiconductor Materials: GaN, AlN, InN, BN, SiC, SiGe*, edited by M. E. Levinshtein, S. L. Rumyantsev, and M. S. Shur (Wiley, New York, 2001).
[33]V. Bougrov, M. Levinshtein, S. Rumyantsev, and A. Zubrilov, *Gallium Nitride (GaN)*, Chapter 1 in *Properties of Advanced Semiconductor Materials: GaN, AlN, InN, BN, SiC, SiGe*, edited by M. E. Levinshtein, S. L. Rumyantsev, and M. S. Shur (Wiley, New York, 2001).
[34]A. Dmitriev and M. Shur, Phys. Status Solidi B **250**, 318 (2013).
[35]Recently, Chilleri *et al.*[36] developed a relaxation-time approximation based formalism in order to examine how the individual scattering processes contribute to the total electron drift mobility. This analytical approach was then used to examine the impact of threading dislocation scattering within the cubic phase of boron nitride.[37] In the analysis of Chilleri *et al.*,[36] the reciprocal of the components of mobility associated with the individual scattering processes was interpreted as being proportional to the scattering rate of that particular scattering process. This suggests that the ballistic mobility expression, i.e., Eq. (7), can be interpreted as being associated with the contacts in an electron device, i.e., that all of the other scattering processes contribute to the bulk mobility, μ_o, and that scattering related to the contacts themselves contribute to the ballistic mobility expression, i.e., Eq. (7), this scattering rate being inversely proportional to the average-time it takes for an electron to transit across the device, where this transit time is essentially $\frac{L}{v}$ with a slight adjustment by a factor, of the order of unity, which takes into account the geometry of the device.
[36]J. Chilleri, Y. Wang, M. S. Shur, and S. K. O'Leary, Solid State Commun. **352**, 114776 (2022).
[37]J. Chilleri, Y. Wang, and S. K. O'Leary, Solid State Commun. **356**, 114925 (2022).
[38]As we recognize that not all materials are expected to be scalable to the level of 1 nm (consider, for example, the 5 nm scale limit that exists for the case of Si[7]), the extension of our results into the short device length range is depicted through the use of dashed lines, this being in recognition of the uncertainty in the underlying physics over this device length range and questions concerning whether or not electron devices, fabricated with these materials, can even be realized at these device length scales. For the purposes of our computations, noting that current work on Si is being performed on devices that are close to its scale limit, we start the dashed line extensions at 5 nm. For the other materials considered in this analysis, as they are less mature materials systems, we start the dashed line extensions at 10 nm.